Preparation of Catalytic Substrates with Ordered Size of Iron Nanoparticles for Production Carbon Nanotubes

Igor Nerush[a], Joe Shapter[a], Jamie Quinton[a], David A.Beattie[b]
[a]School of Chemistry, Physics and Earth Science
Flinders University, Bedford Park, South Australia, 5042
[b]Ian Wark Research Institute,
University of South Australia, Mawson Lakes, SA 5095
Email: Joe.shapter@flinders.edu.au

***Abstract*—A solution of ferrocene in ethanol and acetone was thermally decomposed on silica and porous alumina substrates. The morphology and catalytic activity of the iron nanoparticles produced was investigated.**

Keywords -- carbon nanotubes, catalyst, atomic force microscopy, ferrocene

I. INTRODUCTION

In 1985, Kroto et al. [1] discovered that buckminster fullerene C_{60} has a soccer-ball like symmetrical structure consisting of 12 pentagons and 20 hexagons. This discovery led to an entirely new branch of chemistry [2] and was recognized by the 1996 Nobel Prize in Chemistry [3]. The subsequent discovery of carbon nanotubes by Iijima [4] in 1991 opened up a new era in material science and nanotechnology. Carbon nanotubes are arrangements of carbon hexagons that are formed into tubes. They usually have a diameter ranging from a few angstroms to tens of nanometers and can have lengths of up to several centimeters [5].

Carbon nanotubes are unique nanostructures with remarkable electronic and mechanical properties, some stemming from the close relationship between carbon nanotubes and graphite, and some from their one-dimensional aspects. Initially, carbon nanotubes aroused great interest in the research community because of their exotic electronic structure. As other intriguing properties have been discovered, such as their remarkable electronic transport properties, their unique Raman spectra, and their unusual mechanical properties, interest has grown in their potential use in nanometer-sized electronics and in a variety of other applications [6].

There are a few main techniques of carbon nanotube production such as arc discharge, laser ablation and chemical vapor deposition. For a long time, arc-discharge and laser-ablation have been the principle methods for obtaining nearly perfect SWNT materials, but both of these techniques have disadvantages. In SWNT growth by arc-discharge and laser ablation, typical by-products include fullerenes, graphitic polyhedrons with enclosed metal particles, and amorphous carbon in the form of particles or overcoatings on the sidewalls of nanotubes. Both methods rely on evaporating carbon atoms from solid carbon sources at temperature above 3000 ^{o}C, which is not efficient and limits the scale-up of SWNTs. Finally, the nanotubes synthesised by evaporation methods are in a tangled form that are difficult to purify, manipulate and assemble for building nanoscale structures.

Due to these shortcomings, a third method of SWNT production was developed based on chemical vapour deposition and will be used in this work. The growing process involves heating a catalyst material to high temperatures in a tube furnace and flowing a hydrocarbon gas through a tube reactor for a period of time. Materials grown over the catalyst are collected upon cooling the system to room temperature. The key parameters in nanotube CVD growth are the hydrocarbon used, type of catalyst and growth temperature. The active catalytic species are typically transition-metal nanoparticles formed on a support material such as alumina. The general nanotube growth mechanism in a CVD process involves the dissociation of hydrocarbon molecules catalysed by the transition metal and deposition of carbon atoms on the metal nanoparticle. The precipitation of carbon from the saturated metal particle leads to the formation of tubular carbon solids in sp^2 structure. Tubular formation is favoured over other forms of carbon such as graphitic sheets with open edges because a tube contains no dangling bonds and therefore is in a low energy form.

Currently we are investigating production of CNT by catalytic chemical vapour deposition. There are a few metals that can be used as a catalyst and quite a few substances that can be used as a carbon source. The catalyst can be deposited on surface or added to the gas mixture in chamber. Previous research has shown that size of catalyst nanoparticles is a very important variable in growing carbon nanotubes. The smaller nanoparticles are, the more catalytically active they are. The smaller particles produce better nanotubes in greater quantities.

II. EXPERIMENTAL

We have chosen methane as carbon source, iron as a catalyst, ferrocene as an iron source and preliminary deposition of catalyst on substrate followed by thermal

decomposition of ferrocene. As a template, we are using silica and porous alumina.

Initially, the ferrocene was dissolved in ethanol. Solutions of concentration 1.8, 0.6 and 0.18 %wt. were placed onto substrate. The samples were allowed to dry in air and then treated in a hydrogen atmosphere for 1 hour at 560 ^{0}C. It was found that ferrocene has better solubility in acetone. 5μL of ferrocene solution in acetone with concentration 5%wt., 1%wt., 0.1%wt. and 0.01%wt. was dropped on Si substrate and placed in chamber with 500 ^{0}C for 1 hour in air flow and cooled down in nitrogen flow. In order to remove some potential aggregates the substrates with deposited iron oxide were soaked in acetone for 24 hours, sonicated for two hours and then dried in the air at room temperature.

The synthesis of carbon nanotubes was conducted in a horizontal thermal chemical vapour deposition system by decomposition of CH_4. The as-prepared Fe/Si catalyst was placed in the reaction region of the horizontal quartz-glass tube (inner diameter 1 inch and length 450 mm) heated by electric furnace. The chamber was heated up to 500 ^{o}C. Nitrogen at flow rate 400 ml min^{-1} was applied and ferrocene was decomposed during 20 min. After that, the reactor was heated up to 900 ^{o}C. Prior to deposition reaction, the Fe catalyst was activated for 10 min in ammonia with flow rate 200 mL min^{-1}. The methane was introduced into the chamber with flow rate 100mL min^{-1} and the reaction proceeded for 30 min.

Atomic Force Microscope tapping mode images were taken in air with a multi-mode head and Nanoscope IV controller (Digital Instruments, Veeco, Santa Barbara). Commercially available silicon cantilevers (FESP-ESP series, Veeco probes, Santa Barbara) with fundamental resonance frequency between 70-85 KHz were used. Topographic (height) and amplitude images were obtained simultaneously at a scan rate of 4 – 8 Hz with the parameters of set point, amplitude, scan size, and feedback control optimised for each sample. All images presented represent background subtracted data using the 'flatten' feature in the Digital Instruments software.

X-ray Photoelectron Spectroscopy has been used to confirm the presence of iron on the substrate. X-ray photoelectron spectra were obtained on a Leybold-Heraeus XPS spectrometer equipped with an Al Kα source (1486.6eV). The take-off angle for detection was nominally 90^o from the surface. The pressure in the main chamber was < 5×10^{-8} Torr during analysis

A commercial Raman microscope (Renishaw Ramascope System 1000) was used to collect Raman scattered light. The system consists of a single spectrograph fitted with holographic notch filters and a Peltier cooled CCD detector upon which the Raman spectrum is dispersed. The spectrograph is coupled to a Leica microscope (DMLM) with computer controlled sample stage, rigidly fixed to the spectrograph baseplate. The spectrometer has a maximum lateral resolution of 2 μm and depth resolution of 2 mm. The 785 nm laser (Renishaw-badged compact diode laser) was used for the spectra reported in this work, and was focused onto the sample using a x50 objective (Leica, NA = 0.75). The 785 nm laser delivers around 100 mW of power to the sample and produces a line focus at the sample, increasing the area analysed during acquisition. No smoothing was applied to the spectra.

III. RESULTS AND DISCUSSION

AFM images (Fig. 1) of the silica samples after exposure to ferrocene show an even coverage of nanoparticles on silica surface. A typical XPS spectrum of the exposed surface is shown in Figure 2. The peak at 710 eV belongs to Fe 2p3/2 electrons. This shows that using solution for catalyst preparation is promising.

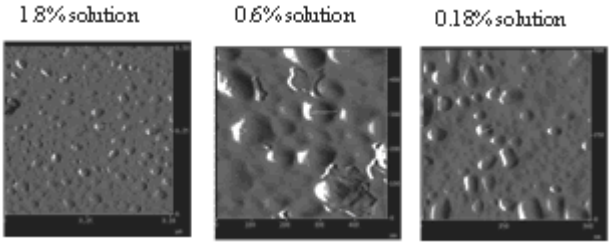

Figure 1. AFM topography images of Fe nanoparticles deposited on Si O_2 from solutions of ferrocene in ethanol with concentration 1.8, 0.6 and 0.18 %wt. respectively.

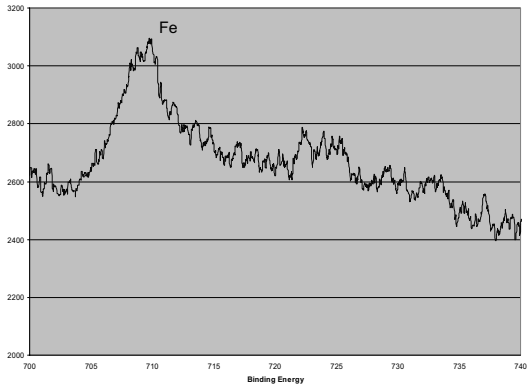

Figure 2. XPS spectra of the Si O_2 catalytic substrate.

The average area of nanoparticles was determined using Nanoscope (R)III Version 5.12b42 software. The results of this analysis are shown in Table 1.

Solution Conc. (%wt)	Mean Nanoparticle Area (nm^2)	Mean Nanoparticle Density (μm^{-2})
1.8	116	1900
0.6	379	700
0.18	179	800

Table 1. Results of Analysis of AFM Images of Nanoparticles Produced on Silica Substrates using Ethanol Solutions

The average size of nanoparticles on each sample are different with no obvious direct correlation between concentration and size. This must mean that there are some other parameters that are important in the dispersion. The most obvious is the quantity of liquid dropped on surface which will effect the depth of liquid and quantity of iron molecules per unit area.

Dissolving the ferrocene in acetone followed by deposition on silica, yields the AFM images shown in Figure 3. These images show a very good coverage of catalyst on silica and an obvious dependence of size and density of nanoparticles on the surface with concentration of solution.

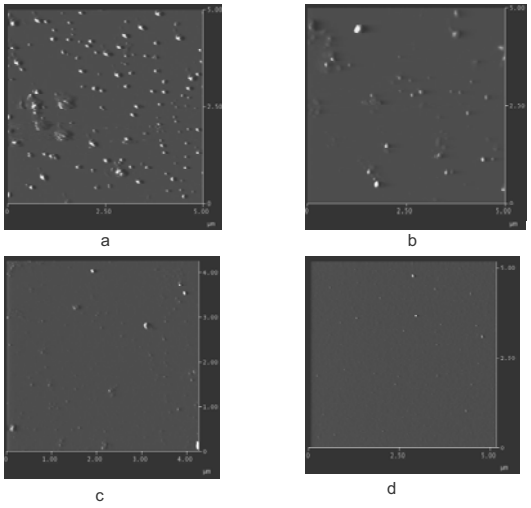

Figure 3. AFM topography images of Fe_2O_3 nanoparticles deposited on Si O_2 from solutions of ferrocene in acetone with concentration (a) 5 %wt., (b) 1 %wt., (c) 0.1 %wt. and (d) 0.01 %wt.

Solution Conc. (%wt)	Mean Nanoparticle Area (nm^2)	Mean Nanoparticle Density (μm^{-2})
5	1371	3524
1	777	949
0.1	684	145
0.01	404	14

Table 2. Results of Analysis of AFM Images of Nanoparticles Produced on Silica Substrates using Acetone Solutions

The AFM image of the grown nanotubes using the catalytically activated silica is shown in Fig. 4. The section analysis shows that diameter of the nanotubes is 15 - 20 nm.

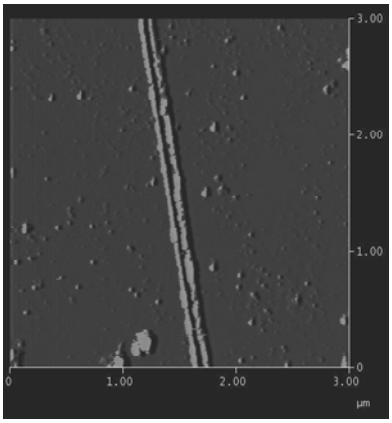

Figure 4. AFM image of SWCNTs.

Raman studies were performed directly on the as-formed carbon nanotubes. The results are shown in Figure 5.

The Raman-allowed tangential mode in graphite is observed at 1582 cm^{-1}, and is called the G mode (from graphite). Unlike graphite, the tangential G mode in SWNTs gives rise to a multi-peak feature, also named the G band, where up to six Raman peaks can be observed in a first-order Raman process. However, a simple analysis can be carried out considering the two most intense peaks that basically originate from the symmetry breaking of the tangential vibration when the graphene sheet is rolled to make a cylindrically shaped tube. The two most intense G peaks are labeled G+, for atomic displacements along the tube axis, and G-, for modes with atomic displacement along the circumferential direction, and the lowering of the frequency for the G- mode is caused by the curvature of the nanotube which softens the tangential vibration in the circumferential direction [7].

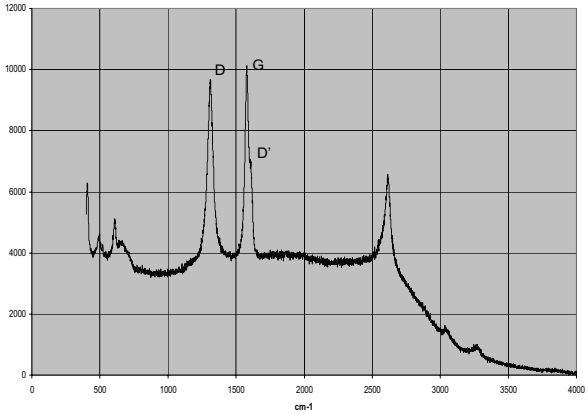

Figure 5. Raman spectra of Si O_2 substrate after carbonisation.

In this case the first-order Raman spectrum (Fig. 5) of carbon nanotubes shows a strong sharp peak at 1580 cm^{-1} (G line), which is the high-frequency E_{2g} first-order mode. One of the most unusual properties of CNTs is that the Raman spectrum shows an additional strong band above1300 cm^{-1} (D line) and a weak band at around 1610 cm^{-1} (D' line). The

strong peak at 1313 cm^{-1} is similar to the peak of pyrolytic graphite which appears at 1340 cm^{-1}. The origin of the D and D' lines in other forms of carbon materials has been explained as disorder-induced features due to the finite particle size effect or lattice distortion [8-10]. In other words, the relative intensity of the 1340 cm^{-1} mode with respect to the 1581 cm^{-1} mode depends on the crystal planar domain size of graphite. In our case it is reasonable that the 1313 cm^{-1} mode origination may be attributed to defects in the curved graphene sheets, tube ends, and finite size crystalline domains of the tubes [11-13]. The appearance of the strong D line of single wall carbon nanotubes can be interpreted as being due to: (1) the turbostratic structure of carbon sheets in tubes, namely the finite size (nanometer order) of the crystalline domains; and (2) the high density of the aligned tubes. Thus, the large amount of crystalline domains on the nanometer scale and the surfaces of the tubes must account for the enhancement of the D line at 1313 cm^{-1}. In principle, the position of the G line at 1580 cm^{-1} is slightly dependent on domain size, but the shift to high frequency is not observed within the experimental accuracy, although the G line at 1581 cm^{-1} appears to be a doublet due to the finite size effect. The D line (at 1313 cm^{-1}) has also been attributed to first-order scattering from a zone–boundary phonon activated by the disorder associated with finite crystalline size. This assignment is corroborated with the strong peak at 2620 cm^{-1} (i.e., ~2 × 1313 cm^{-1}) in the second-order Raman spectrum. While the D line at 1313 cm^{-1} has a counterpart in the second-order spectrum, if its presence results from the finite crystalline size of nanometer order, it might be expected that the peak at 1610 cm^{-1} also has a counterpart in the second-order spectrum of CNTs, namely, 3281 cm^{-1}. It is important to note that the differences in frequency between the observed first-order modes and half the frequency of the corresponding second order modes could be due to matrix element effects or to the region of the k space strongly sampled by the breakdown of wave–vector conservation.

The peak at 2620cm^{-1} (D*) is the overtone of the D line, and the peak at 3049 cm^{-1} is attributed to the combination of the D and G lines. The observation of the line at 3281 cm^{-1} is strong evidence for overtone scattering from the highest-frequency line at ~1610 cm^{-1} in the density of states (14).

Similar experiments using porous alumina substrate have also been done. In this case, a thick black deposited was obtained. This black sediment was dissolved in DMF and dispersed onto mica and analysed by AFM (Fig. 6). The diameter of the produced nanotubes is about 2.5 nm.

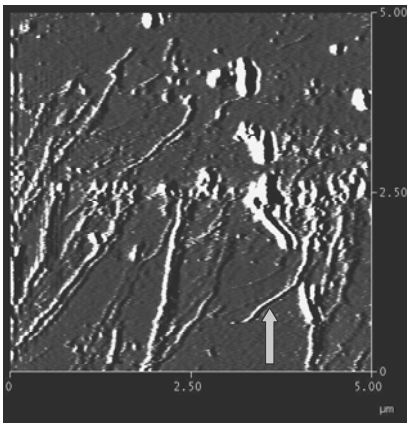

Figure 6. AFM image of deposit grown on alumina substrate. Image was obtained using a mica substrate.

In summary, we have successfully prepared catalytic substrates with different densities of iron nanoparticles and synthesised single wall carbon nanotubes. The tubes are around 15–20 nm in diameter. Raman spectra up to second order of the SWCNTs have been collected, indicating that the tubes are highly graphitised. The appearance of a strong D band shows that a nanometer scale turbostratic structure may be formed in carbon nanotubes due to the relatively low growth temperature. The Raman studies are consistent with the results from AFM.

IV. REFERENCES

[1] L.Dai and A.W.H.Mau, Adv.Mater., 2001. 13(12 -13).

[2] H.W.Kroto, A.W.Allaf, S.P.Balm, Chem. Rev. 1991, 91, 1213.

[3] R.Baum, Chem. Eng. News 1996, 74(42), 7

[4] S.Iijima, Nature 1991, 354, 56.

[5] M.S.Dresselhaus, G.Dresselhaus, P.Eklund, Science of Fullerenes and Carbon Nanotubes, Academic, San Diego, CA 1996.

[6] M.S.Dresselhaus, G.Dresselhaus, Ph.Avouris Carbon nanotubes: synthesis, structure, properties, and applications (Springer, Berlin, Heidelberg 2001)

[7] A.Jorio, M.A.Pimenta, A.G.Souza Filho, R.Saito, G.Dresselhaus, M.S.Dresselhaus, New J. of Phys., 2003, 5, 139.1–139.17.

[8] G.Vitali, M.Rossi, M.L.Terranova, V.Sessa, J. Appl. Phys., 1995, 77, 4307.

[9] D.G.McCulloch, S.Prawer, A.Hoffman, Phys. Rev., 1994, B 50, 5905.

[10] V.Barbarossa, F.Galluzzi, R.Tomaciello, A.Zanobi, Chem. Phys.Lett., 1991, 185, 53.

[11] F.Tuinstra, J.L.Koenig, J. Chem. Phys., 1970, 53, 1126.

[12] R.J.Nemanich, S.A.Solin, Phys. Rev. B, 1979, 20, 392.

[13] R.Tsu, J.H.Gonzalez, I.G.Hernandez, Solid State Commun., 1978, 27, 507.

[14] W.Li, H.Zhang, C.Wang, Y.Zhang, L.Xu, K.Zhu, S.Xie, Appl. Phys. Lett., 1997, 70(20), 2684-2686.